# Decay of the r-process nuclides ^{137,138,139}Sb, and the A=130 solar r-process abundance peak

O. Arndt, K.-L. Kratz, W. B. Walters, K. Farouqi, U. Köster, V. Fedosseev, S. Hennrich, C. J. Jost, A. Wöhr, A. A. Hecht, B. Pfeiffer, J. Shergur, and N. Hoteling

Phys. Rev. C **84**, 061307 — Published 28 December 2011

DOI: 10.1103/PhysRevC.84.061307

**Decay of the r-process nuclides $^{137,138,139}$Sb and the A = 130 solar r-process abundance peak**

O. Arndt, [1] K.-L. Kratz, [1] W. B. Walters, [2] K. Farouqi, [1] U. Köster, [3] V. Fedosseev, [4] S. Hennrich, [1] C. J. Jost, [1] A. Wöhr, [2,5] A. A. Hecht, [2,5] B. Pfeiffer, [1] J. Shergur, [2,5] and N. Hoteling [2,5]

[1] *Max-Planck-Institut für Chemie, Otto-Hahn-Institut, Joh.-J. Becherweg 27, D 55128 Mainz, Germany*

[2] *Department of Chemistry and Biochemistry, University of Maryland, College Park, Maryland 20742, USA*

[3] *Institut Laue-Langevin, F-38042 Grenoble, France*

[4] *CERN, CH-1211 Geneva 23, Switzerland*

[5] *Physics Division, Argonne National Laboratory, Argonne, Illinois 60439, USA*

Half- life ($T_{1/2}$) and $\beta$-delayed neutron branching ($P_n$) values of 492(25) ms and 49(8)%, 350(15) ms and 72(8)%, and 93(13) ms and 90(10)% for the r-process nuclei $^{137,138,139}$Sb, respectively, have been measured at CERN/ISOLDE by counting $\beta$-delayed neutrons. More precise $T_{1/2}$ and $P_n$ values of 300(15) ms and 27(4)%, and 273(7) ms and 50(8)% for $^{136,137}$Sn, respectively, have also been measured. The sources were prepared by using the selective ionization of Sb or Sn with the Resonance Ionization Laser Ion Source and the High-Resolution Mass Separator. The new data for Sb isotopes are compared with calculated $T_{1/2}$ and $P_n$ values for both spherical and non-spherical shapes. The data have been incorporated into parameterized nucleosynthesis calculations of the r-process in high-entropy winds of core-collapse supernovae in order to study the properties of the $A$ = 130 Solar-System r-process abundance peak.

PACS number(s): 21.10.Tg, 23.40.-s, 26.30.Hj, 27.60.+j

The ability to correctly reproduce the $A$ = 130 Solar-System (SS) isotopic r-process abundance peak, which acts as the main bottleneck in the r-process matter flow, has served as a key test of nucleosynthesis models designed to calculate the total SS r-abundance pattern [1-8]. The quality and usefulness of such calculations have been aided over the past 15 years by the use of newly measured experimental values for a number of the isotopes of Ag, Cd, In, and Sn that lie directly in the path of the r-process. Many of those data have been obtained at CERN/ISOLDE through the use of Resonance Ionization Laser Ion Sources (RILIS) to obtain elemental selectivity, in conjunction with high-resolution mass separation to isolate specific isotopes. During that period -- with the continuous development and use of RILIS -- nuclear-structure properties of about 25 r-process relevant isotopes in the $A \sim 130$ mass region have been measured including half-lives of 46(7), 158(60), and 35(10) ms for $^{129g,129m,130}$Ag, respectively, 242(8), 104(6), 162(7), 68(3), 95(10), and 57(10) ms for $^{129g,129m,130,131,132,133}$Cd, respectively, and half-lives of 206(6), 165(3), 141(5), and 92(10) ms for $^{132,133,134,135}$In, respectively [9-14]. In this paper new values are reported for the half-lives of $^{137,138,139}$Sb obtained through the use of the RILIS tuned for ionization of Sb. More precise half-lives for $^{136,137}$Sn are also reported. The use of these chemical ionization and mass-separation techniques for the study of Sn, Sb, and Te, nuclei with $A > 130$ is hindered by the increasingly large numbers of $\beta$-delayed neutrons ($\beta$dn) plus $\beta$ and $\gamma$ radiations arising from Cs isotopes that are easily ionized, making $\beta$ counting for $P_n$ value determinations increasingly difficult. All these experimental data plus optimized theoretical $\beta$-decay properties, calculated with the quasi-particle random-phase approximation (QRPA), have been incorporated into parameterized dynamical nucleosynthesis calculations within the so-called high-entropy-wind (HEW) scenario of core-collapse supernovae (for details of the nucleosynthesis model used, see e.g. Refs. [4] and [7]). In particular, the formation of the $A$ = 130 r-process abundance peak has been investigated with this model.

The half-lives were determined by measuring the time dependence of $\beta$dn from the Sb parent isotopes using the Mainz Neutron Long Counter in an experimental setup that has been described by Hannawald *et al*. [15], Kautzsch *et al*. [16], and Shergur *et al* [17]. A new scheme for ionization of Sb was developed at ISOLDE for this experiment. [18,19]. As proton beam pulses from the Proton Synchrotron Booster (PSB) arrive in intervals of 1.2 s, data collection was set to cover a time range of 2048 ms or longer, and to utilize at most every other PSB pulse. The clock for the data collection system was reset by the arrival of a new PSB pulse. The frequency and time range for sample collection and were varied to produce sources of reasonable strength and to facilitate the determination of counting rates for the longer-lived isotopes that grew in from radioactive decay of the Sb nuclei and to measure background decay rates.

The $\beta$dn counts were binned into 5-ms time intervals, and plotted against the time after the PSB pulse, as shown in Fig. 1 for $A$ = 137 with the laser on, and with the laser off. The counts observed with the laser off arise largely from the decay of $^{137}$I, produced by surface ionization, that is also a $\beta$dn emitter with a 24.1(1)-s half–life and a 7.0(5)% $P_n$ value [20-23]. Similar backgrounds are found at A = 138 and 139 from 6.49(7)-s $^{138}$I ($P_n$ = 5.2(4)%) and 2.28(1)-s $^{139}$I ($P_n$ = 10.8(12)%). The differences between the counts per time interval obtained with the laser on minus the counts observed with the laser off are subjected to a two-component fit that includes growth and decay of a $^{137}$Te component with a $P_n$ value of 3.0(2)%. This fit yields a half-life of 492(25) ms. These values are consistent with those reported by Shergur *et al.* of 450(50) ms and a $P_n$ of 49(10)% that emerged from fitting the neutron decay curve for $^{137}$Sn decay [24].

The differences between the counts per time interval obtained with the laser on minus the counts observed with the laser off for $^{138}$Sb decay are shown in Fig. 2. The fitting process for these data is simplified by the low $P_n$ values and relatively long half-life values for the daughter $^{137,138}$Te activities. Using half-life and $P_n$ values of 2.5 s and 3.0% for $^{137}$Te, respectively, and 1.4 s and 6.3% for $^{138}$Te, respectively, a three-component fit for $^{138}$Sb decay yields a half-life of 350(15) ms and a $P_n$ value of 72(8)%.

The difference data for $^{139}$Sb decay are shown in Fig. 3. The yield for $^{139}$Sb is far lower than for $^{138}$Sb, but sufficient to extract a half-life of 93(13) ms with a 14% uncertainty. A three-component fit that included only the 1.4-s $^{138}$Te daughter and the 6.3-s $^{138}$I granddaughter arising from the $\beta$dn decay of the parent $^{139}$Sb yielded a 93-ms half-life. That value is identical (within uncertainties) to a five-component fit that also included 1.6(3)-s $^{139}$Te and 2.28-s $^{139}$I. The conclusion is that the $P_n$ value for $^{139}$Sb is of the order of 90(10)%.

Subsequent to the experiment in which the half-lives of 250(30) and 190(60) ms were reported for $^{136,137}$Sn, respectively, it has been possible to obtain significant improvements in the reduction of background activities at ISOLDE that contribute to the observed spectra [24]. The difference data for $^{137}$Sn arising from a new measurement with the RILIS set for Sn achieved a much lower "laser-off" background are shown in Fig. 4. Using the newly measured half-life of 492(25) ms for daughter $^{137}$Sb, a somewhat longer and more precise half-life of 273(7) ms is extracted from these data for $^{137}$Sn, along with a $P_n$ value of 50(10) %. A longer half-life of 300(15) ms has also been determined for $^{136}$Sn, with a $P_n$ value of 27(4)%.

These results emphasize the importance of actual measurements for half-lives of nuclei that are expected to be relevant for r-process nuclei that lie near closed shells. At the outset of the experiment, the indirectly determined half-life for $^{137}$Sb was 450(60) ms, which turns out to be reasonable with respect to the new value of 492(25) ms [12]. In contrast, earlier QRPA calculations based on the finite-range droplet model (FRDM) masses that only included Gamow-Teller (GT) transitions in the determination of $\beta$ strength distribution yields predictions of 1050 ms, 41 ms and 179 ms, for the half-lives of $^{137,138,139}$Sb, respectively, far different from the observed half-lives [25].

The half-lives and $P_n$ values for the neutron-rich Sb nuclei are listed in Table I, along with recently calculated values that include both Gamow-Teller (GT) and first-forbidden (ff) transitions. Literature data for $^{134}$Sb isomers are included for comparison with the values for $^{136,138}$Sb [26]. The details of these QRPA(GT+ff) calculations are described by Möller,

Pfeiffer and Kratz [27]. The results demonstrate the effects of the possibility of low- and high-spin isomers in odd-odd nuclei. For example, the calculated half-life for $^{134}Sb_{83}$ of ~7 s is reasonably close to the measured value for the 10.07(5) s $7^-$ isomer, and a factor of 10 too long for the decay of the $0^-$ ground state. The calculated $P_n$ value for $^{134}Sb_{83}$ is also consistent with decay of a long-lived, high-spin isomer. For $^{136}Sb_{85}$ the half-life calculated with non-zero collectivity ($\varepsilon_2 = +0.033$) is 20% larger than the observed value, compared to the spherical calculation ($\varepsilon_2 = 0.0$) that yields a half-life longer by a factor of ~2. For $^{138}Sb_{87}$, the calculation with non-zero collectivity indicates a low-spin ground state with an open $\beta$-decay channel to the ground state of $^{138}$Te, whereas the calculation with zero collectivity reflects the expectation of a rather high-spin state, perhaps as high as $8^-$ whose direct $\beta$ decay to lower-energy levels is hindered. The measured value indicates a medium-spin ground state. For $^{135}Sb_{84}$, collectivity does not appear to play a role, as both calculations, one with $\varepsilon_2 = 0.0$ and the other with $\varepsilon_2 = -0.008$ yield half-lives that are a factor of 2 too long. For both $^{137,139}Sb_{86,88}$, the calculated values using $\varepsilon_2 = +0.050$ and +0.092, respectively for the Sb parent are slightly larger than the measured values, but within reason in view of the universal scope of the calculations as seen in Table I. These data show that collectivity, as included in the model via non-zero values for $\varepsilon_2$, becomes important above $N = 84$, as the half-lives calculated in non-zero collectivity tend closer to the observed values, in contrast with those calculated with $\varepsilon_2 = 0.0$.

Table I. Measured and calculated half-lives and $P_n$ values for neutron-rich Sb nuclei.

| Neutron number | 83 | 84 | 85 | 86 | 87 | 88 | 89 |
|---|---|---|---|---|---|---|---|
| Isotope | $^{134}Sb_{83}^{g}/^{134}Sb_{83}^{m}$ | $^{135}Sb_{84}$ | $^{136}Sb_{85}$ | $^{137}Sb_{86}$ | $^{138}Sb_{87}$ | $^{139}Sb_{88}$ | $^{140}Sb_{89}$ |
| Half-life (ms) | 780(60)/10070(50) | 1679(15) | 923(14) | 492(25) | 350(15) | 93(+14/-3) | |
| $P_n$ (%) | 0.0/0.088(4) | 22(3) | 16(3) | 49(8) | 72(8) | 90(10) | |
| Calculated $T_{1/2}$ ($\varepsilon_2 = 0.0$) (ms) | 7490 | 3327 | 2000 | 1265 | 565 | 495 | 364 |
| Calculated $T_{1/2}$ ($\varepsilon_2 \neq 0.0$) (ms) | 6960 | 3301 | 1103 | 603 | 423 | 150 | 37 |
| Calculated $P_n$ ($\varepsilon_2 = 0.0$) (%) | 0.12 | 33 | 40 | 56 | 69 | 87 | 78 |
| Calculated $P_n$ ($\varepsilon_2 \neq 0.0$) (%) | 0.12 | 34 | 46 | 76 | 73 | 96 | 62 |

As the exact astrophysical site and stellar conditions of the r-process are still uncertain, detailed exploration of the systematics of this important nucleosynthesis process in terms of its dependence on nuclear-physics properties far from $\beta$-stability remains a critical area of investigation. A particularly important mass region in this context is that of the $A$ ~130 r-process abundance peak, which, owing to the $N$ =82 magic neutron-shell closure, is the dominant bottle-neck in the total r-process matter flow. In the past, the majority of such r-process studies have been related to the widely site-independent, classical "waiting-point" approach [28]. In that model the r-process matter flow has been studied under rather simplistic astrophysical conditions, assuming an overall $(n,\gamma) = (\gamma,n)$ equilibrium with several local $\beta$-flow equilibria, a constant stellar temperature $T$, and constant neutron densities $n_n$ in the superpositions of the different $n_n$ components, as well as an instantaneous freezeout [1,5,6,29-31].

Already in the early 1990's, Kratz *et al*. [1], and Thielemann *et al*. [31], pointed out several crucial items for systematic r-process explorations: (i) the potential challenge of learning nuclear structure far from $\beta$-stability from r-process abundances; (ii) wherever possible, the avoidance of inconsistent sources of nuclear-physics properties; and (iii) the conjecture of a local overestimation of the $N$=82 shell strength below doubly-magic $^{132}$Sn in the FRDM mass model. Guided and motivated by these results, not only has a considerable effort been focused on developing new experimental techniques to identify a large number of new, r-process relevant isotopes (the majority of them in the $A$ ~ 130 mass

region), but also to test in great detail the possible impact of different theoretical models for nuclear masses and gross β-decay properties. The resulting information has been reported in a wide range of publications [1,4-7,14 27,29-31,33,34].

As a consequence of this work, in more recent years a completely model-consistent nuclear-physics input for the quantities of $Q\beta$, $S_n$, $T_{1/2}$(GT+ff), $P_{xn}$(GT+ff) and neutron-capture cross sections deduced from the quenched version of the deformed mass model ETFSI has been used [5,7,30-34]. For comparison, the analogous model-consistent nuclear input from the FRDM mass model, [4-7,25,27,31] and occasionally different versions of the HFB model (up to HFB 17) as well as the Duflo-Zuker mass formula have also been used [38,39].

To illustrate the impact of the new experimental data, the optimized r-process abundance data are plotted in Fig. 5, along with the calculated r-process yields using recently updated input data, as well as with yields calculated using data that were available and in use ~ ten years ago, using EFSI-Q masses and first-forbidden β decay [36]. Notice that in this graph the r-abundances have been normalized to the r-only isotope, $^{128}$Te, (in contrast to the often-used normalization to the r-only isotope $^{130}$Te) and a linear abscissa has been used where a factor of 2 difference stands out more sharply than in plots that use logarithmic abscissas, see, for example the plots in refs (5-7,30]. The SS-r isotopic abundance breakdown has been deduced from the recent total SS abundance evaluation of Lodders, Palme & Gail [40] and the new s-process contributions communicated by Gallino [41]. For the current calculated isotopic r-process abundance data shown for the $A$ = 130 peak in Fig. 5, the consistent nuclear-physics input based on the quenched mass model ETFSI-Q [35,36] has been used, and two additional improvements in the nuclear-physics input have been incorporated for the first time. First is the inclusion of the $\beta$-decay half-lives of the known $\pi p_{1/2}$ isomers in addition to the $\pi g_{9/2}$ ground-state decays in the two $N$ = 82 odd-proton nuclei $^{131}$In and $^{129}$Ag [10,12,14,42], complemented by theoretical predictions for the lower-$Z$ isotopes $^{125}$Rh to $^{123}$Tc [43]. The second corresponds to new QRPA(GT+ff) calculations for the local mass region of exotic 83 < $N$ < 87 r-process isotopes between $Z$ = 42 Mo and $Z$ = 48 Cd [43]. In these calculations using a spherical Nilsson / BCS model, the relevant κ and μ parameters were optimized to reproduce the experimental level structures of $^{130}$In [13] and, in particular, $^{131}$In [11,12]. This updated scenario now includes a piece by piece replacement of earlier nuclear-physics input, as well as a change from parameter studies within the site-independent waiting-point model to dynamical calculations within the more realistic, site-specific astrophysical process of the neutrino driven or HEW ejecta of core-collapse supernovae, first suggested in refs [44-46], with time variations in neutron density $n_n$, stellar temperature $T$ and matter density $\rho$, and a detailed treatment of the whole freezeout phase [4,7,43]. As is evident from Fig. 5, with the current best possible input of nuclear data and the choice of appropriate astrophysical conditions for the SN-II HEW scenario, a satisfactory reproduction of the SS r-process isotopic abundance "residuals" of the 2nd r-process peak is possible. Particular attention is drawn to the odd-even effect seen in the r-process "residuals" that is reasonably reproduced in the calculations.

In contrast to the new fit of the r-abundance peak, it can be seen that the use of the older nuclear-physics input data, for example still used recently by Farouqi et al. [7] in the current HEW model, has led to a less satisfactory overall agreement with the SS r-process -"residuals". In particular, with the old data the abundances in the rising wing of the peak were overestimated by an average factor of 1.9, whereas the 129 ≤ A ≤ 132 region was underproduced by an average factor of 2.3. Now, with the new nuclear-physics data input, the mass shift in the left wing of the peak is reduced, and the local underabundances at the top of the peak are filled up. Both improvements in the new abundance calculations arise from (i) the longer "stellar" half-life of $^{129}$Ag (by considering the effect of the $T_{1/2}$ ~ 160 ms of the $\pi_{1/2}$ isomer [10] and the new theoretical $P_{xn}$ values of the most important HEW r-process progenitor isotopes in the 130 < A < 134 mass region, such as $^{130-132}$Pd, $^{130-133}$Ag, and $^{133,134}$Cd [43].

In summary, the $\beta$-decay half-lives and $\beta$dn branching ratios of neutron-rich r-process $^{137,138,139}$Sb nuclei have been measured by counting $\beta$–delayed neutrons from Sb samples ionized by the ISOLDE resonance ionization laser ion source, and isolated by the high-resolution mass separator. The data from these new measurements have been combined

with those from previous measurements to provide experimental half-lives for many of the key r-process waiting-point nuclei associated with the $A$ = 130 abundance peak. As a consequence, it is now possible to provide a reasonable fit to both the position and width of the $A$ = 130 abundances as well as much of the odd-even staggering on the high-$A$ side of the peak. Both the peak position and width are crucial to the subsequent reproduction of the rare-earth pigmy peak, the third r-process peak at A = 195 and the U and Th chronometers. The results of dynamical calculations for isotopic r-process abundances after decay back to $\beta$-stability, as expected in the HEW scenario of core-collapse SN-II are presented and found in good agreement with the observed SS r-"residuals" for the choice of medium neutron freezeout temperatures of $T_9 \sim 0.85$ and wind velocities of $V_{exp} \sim 7500$ km/s. Such astrophysical conditions are essential for the further r-process matter flow to the rare-earth element pygmy-peak region up to a simultaneous correct fit of the properties of the third r-abundance peak at $A \sim 195$ (for details, see e.g. Ref. [7]). Finally, when converting the isotopic r-abundances into elemental abundances, as usually measured in metal-poor halo stars [46-50], a reliable reproduction of their abundance patterns for the "main" r-process beyond Ba up to the actinide cosmochronometers, can, at present, be fully obtained with parameterized nucleosynthesis calculations as outlined in Ref. [7] and used in the present paper [51].

This work was supported by the U.S. Department of Energy under Grant DE-FG02-94-ER40834, and the Bundesministerium für Bildung and Forschung (BMBF) under contract 06MZ-864. The authors wish to acknowledge the support of the ISOLDE staff during the experiments, and during the development of the ionization scheme for Sb. W. B. Walters also wishes to acknowledge the support of the Alexander von Humboldt Foundation.

[1] K.-L. Kratz *et al*., Astrophys. J. **403**, 216 (1993)
[2] K. Takahashi, J. Witti, and H.-T. Janka, Astron. Astrophys. **286**, 857 (1994).
[3] B. S. Meyer, J. Phys. G **19**, 197 (1993).
[4] C. Freiburghaus, *et al*., Astrophys. J. **515**, 381 (1999).
[5] K.-L. Kratz, *et al*., Astrophys. J. **662**, 39 (2007).
[6] B. Pfeiffer *et al*., Nucl. Phys. **A693**, 282 (2001).
[7] K. Farouqi *et al*., Astrophys. J. **712**, 1359 (2010).
[8] A. Arcones and G. Martinez-Pinedo, Phys. Rev. C **83**, 045809 (2011).
[9] I. Dillmann *et al*., Phys. Rev. Lett. **91**, 162503 (2003).
[10] K.-L. Kratz *et al*., Eur. Phys. J. A Supplement **1**, 633 (2005) doi: 10.1140/epjad/i2005-06-157-2.
[11] M. Hannawald *et al*., Phys. Rev. C **62**, 054301(2000).
[12] O. Arndt *et al*., Acta Phys. Pol. B **40**, 437 (2009).
[13] I. Dillmann *et al*., Eur. Phys. J. A **13**, 281 (2002).
[14] K. Kratz *et al*., Hyperfine Interactions **129**, 185 (2000).
[15] M. Hannawald *et al*., Phys. Rev. Lett. **82**, 1391 (1999).
[16] T. Kautzsch *et al*., Eur. Phys. J. A **9**, 201 (2000).
[17] J. Shergur *et al*., Phys. Rev. C **71**, 064321 (2005).
[18] R. Catherall *et al*., Rev. Sci. Instrum. **75**, 1614 (2004).
[19] V. N. Fedosseev *et al*., Hyperfine Int. (2005) DOI 10.1007/s10751-005-9204-2
[20] B. Pfeiffer, K.-L. Kratz, and P. Möller, Prog. Nucl. Energy **4**, 39, 2002).
[21] E. Browne and J. K. Tuli, Nucl. Data Sheets **108**, 2173 (2007).
[22] A. A. Sonzogni, Nucl. Data Sheets **98**, 515 (2003).
[23] T. W. Burrows, Nucl. Data Sheets **92**, 623 (2001).
[24] J. Shergur *et al*., Phys. Rev. C **65**, 034313 (2002).
[25] P. Möller, R. Nix, and K.-L. Kratz, At. Data Nucl. Data Tables **66**, 131 (1997).
[26] A. A. Sonzogni, Nucl. Data Sheets **103**, 1 (2004).
[27] P. Möller, B. Pfeiffer, and K.-L. Kratz, Phys. Rev. C **67**, 055802 (2003).
[28] E. M. Burbidge *et al*., Rev. Mod. Phys. **29**, 547, (1957).
[29] F.-K. Thielemann *et al*., Prog. Part. Nucl. Phys. **46**, 5 (2001).
[30] K.-L. Kratz, K. Farouqi, and B. Pfeiffer, Prog. Part. Nucl. Phys. **59**, 147 (2007).
[31] F.-K. Thielemann *et al*., Nucl. Phys. **A570**, 329 (1994).
[32] P. Möller *et al*., At. Data Nucl. Data Tables **59**, 185 (1995).
[33] B. Chen *et al*., Phys. Lett. **B355**, 37, (1995).
[34] K.-L. Kratz *et al*., AIP Conf. Proc. **819**, 409 (2006); **972**, 298 (2008).

[35] J. M. Pearson, R. C. Nayak, and S. Goriely, Phys. Lett. **B387**, 455 (1996).
[36] P. Möller, and K.-L. Kratz, Table of half-life and $P_n$ values QRPA, ETFSI-Q, unpublished 2002).
[37] Y. Aboussir *et al*., At. Data Nucl. Data Tables **61**, 127 (1995).
[38] S. Goriely, N. Chamel, and J. M. Pearson, Phys. Rev. Lett. **102**, 152503 (2009).
[39] J. Duflo and A. P. Zuker, Phys. Rev. C **52**, R23 (1995).
[40] K. Lodders, H. Palme and H.-P. Gail; Landolt Börnstein. New Series VI/4B, 4.4, Springer 34 (2009).
[41] R. Gallino, private communication, 2009.
[42] Yu. Khazov *et al*., Nuclear Data Sheets **107**, 2715 (2006).
[43] K.-L. Kratz and K. Farouqi, to be published.
[44] S. E. Woosley and R. D. Hoffman, Astrophys. J. **395**, 202 (1992).
[45] B. Meyer *et al*., Astrophys. J. **399**, 656 (1992).
[46] S. E. Woosley *et al*., Astrophys. J. **433**, 229 ( 1994).
[47] I. U. Roederer *et al*., Astrophys. J. **698**, 1963 (2009).
[48] K.-L. Kratz *et al*., New Astron. Rev **48**, 105 (2004).
[49] J. J. Cowan and C. Sneden, Nature **440**, 1151 (2006).
[50] C. Sneden, J. J. Cowan, and R. Gallino, Rev. Astron. Astrophys. **46**, 241 (2008).
[51] A. Frebel and K.-L. Kratz, IAU Symp. **258**, 448 (2008).

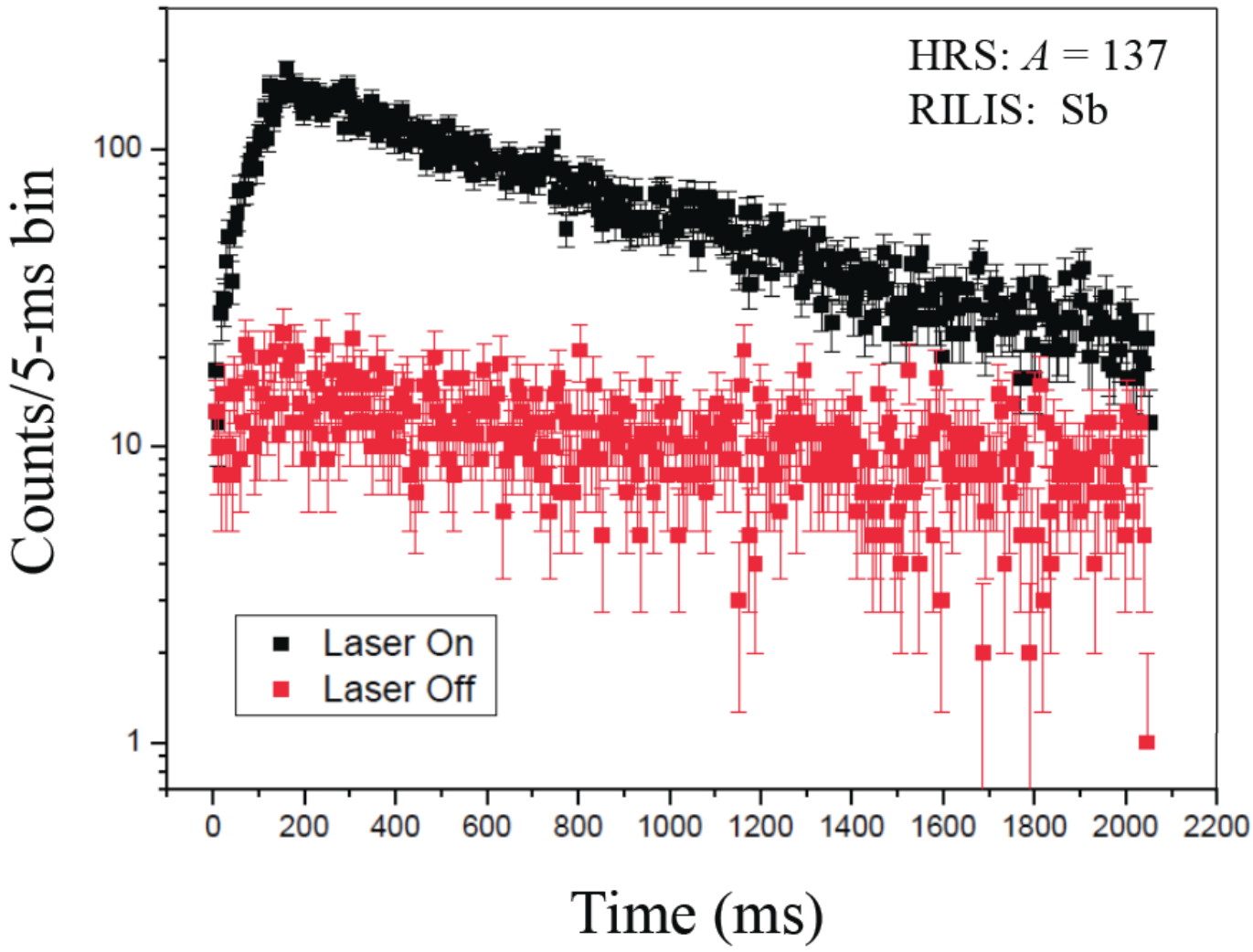

Figure 1. (Color online) Counts per 5 ms time bin plotted versus the time following a proton pulse from the PSB with the HRS set for $A$ = 137. The upper curve (black on-line) shows data taken with the laser on, and the lower curve (red on-line) shows data taken with the laser off.

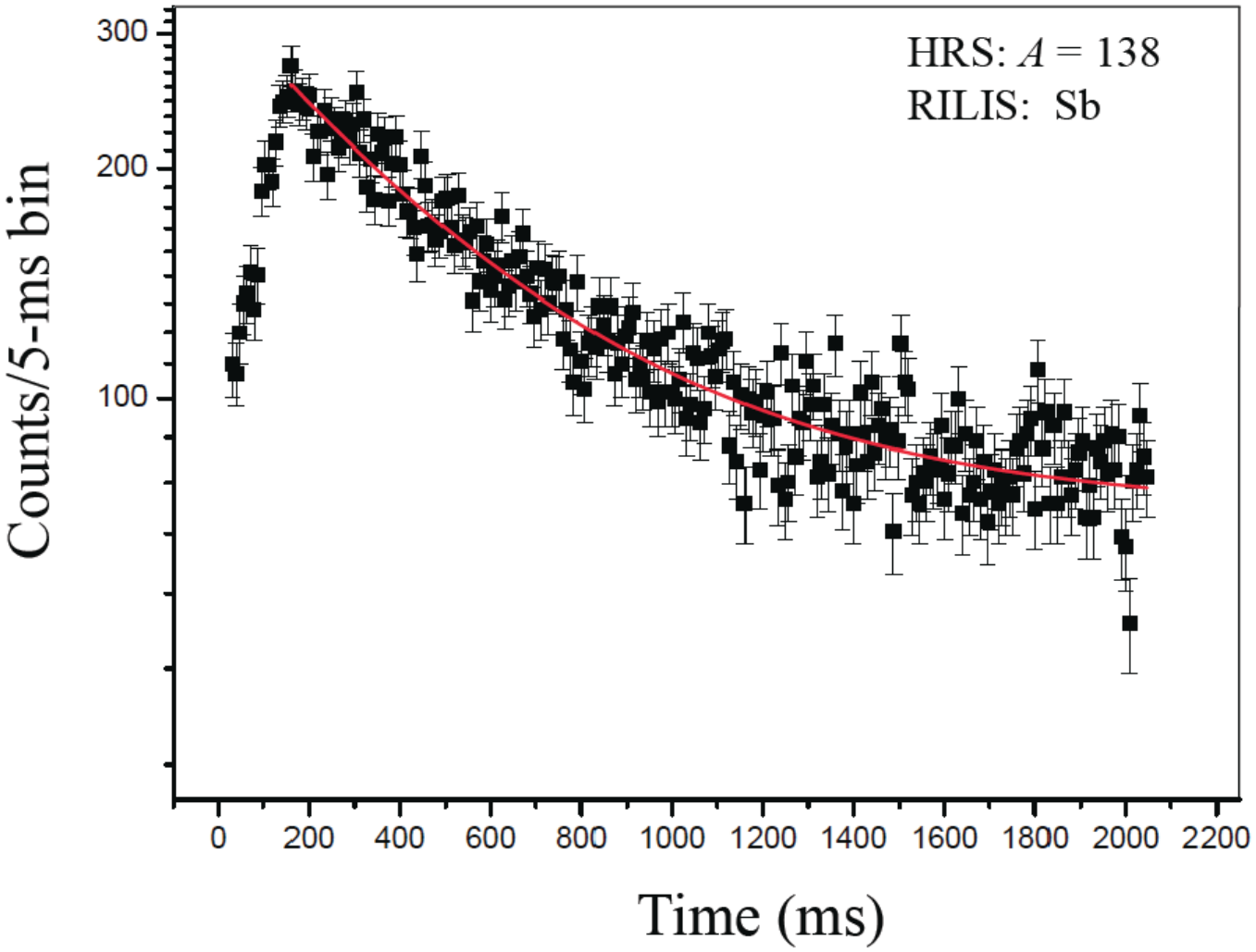


Figure 2. (Color online) Difference per 5 ms time bin between the counts observed with the laser on and the laser off, plotted versus the time following a proton pulse from the PSB with the HRS set for $A$ = 138. The solid line (red on-line) is a three-component fit to the data yielding a half-life of 350(15) ms.

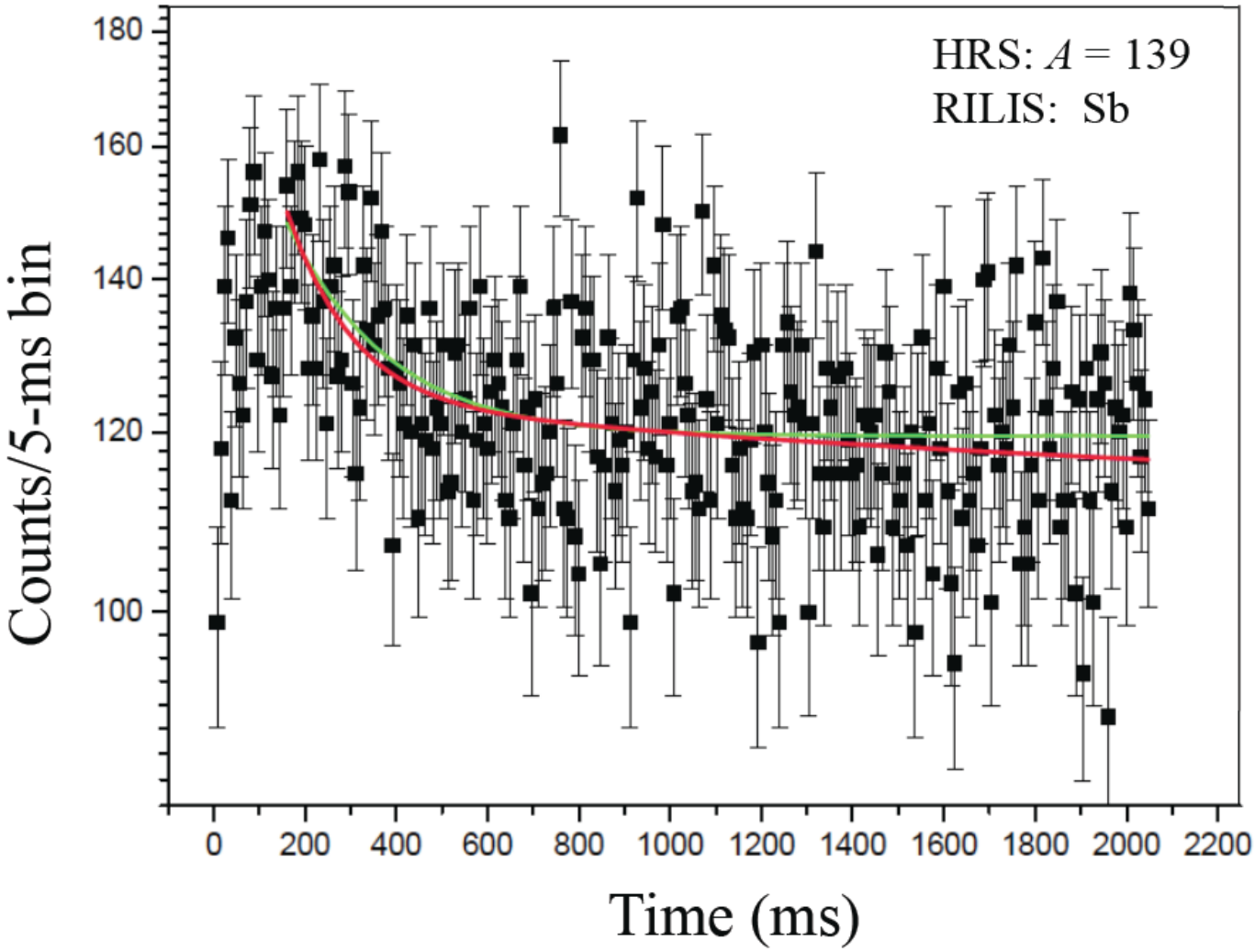


Figure 3. (Color online) Difference per 5 ms time interval between the counts observed with the laser on and the laser off, plotted versus time following a proton pulse from the PSB with the HRS set for $A = 139$. The solid [thin] line (green on-line) is a single component fit plus background to the data yielding a half-life of 144 ms. The thicker line (red on-line) shows a five-component fit that yields a half-life of 93(13) ms.

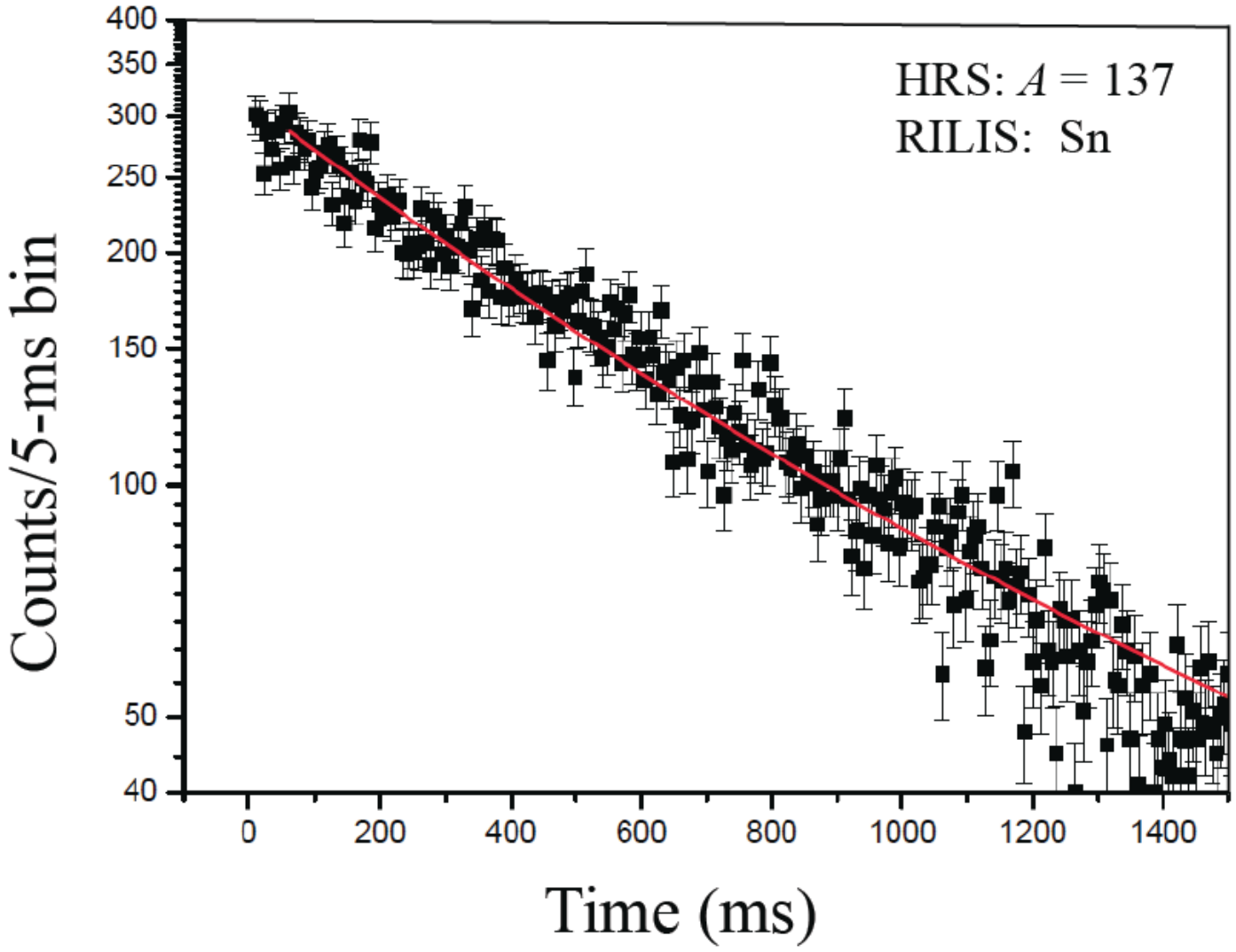


Figure 4. (Color online) Difference per 5 ms time interval between the counts observed with the laser on and the laser off, plotted versus the time following a proton pulse from the PSB with the HRS set for $A$ = 137 and the laser set to ionize Sn. The solid line (red on-line) shows a three-component fit that yields a half-life of 273(7) ms.

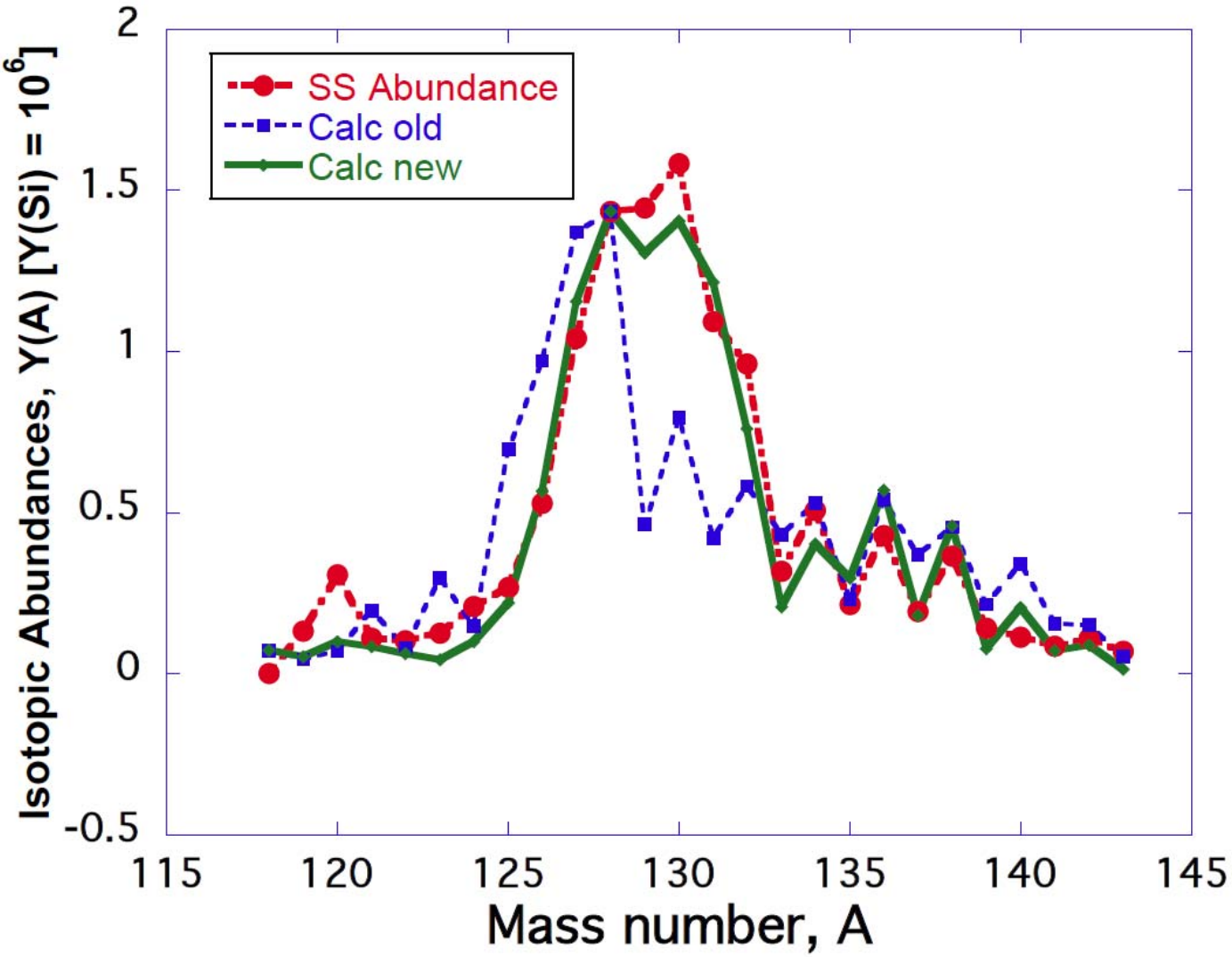


Figure 5. (Color online) Observed r-process residual isotopic abundances (red online) along with the values calculated as described in the text using updated half-lives and $P_n$ values (green online) , and older half-lives and $P_n$ values (blue online). The calculated values are normalized to the abundance of 1.435 for $^{128}$Te.